Cell Transplantation, Vol. 21, pp. 1969–1984, 2012

0963-6897/12 $90.00 + .00
DOI: http://dx.doi.org/10.3727/096368912X647252
E-ISSN 1555-3892
www.cognizantcommunication.com

Alginate Scaffolds for Mesenchymal Stem Cell Cardiac Therapy: Influence of Alginate Composition

Caroline Ceccaldi,*† Sophie Girod Fullana,* Chiara Alfarano,† Olivier Lairez,† Denis Calise,† Daniel Cussac,†‡ Angelo Parini,†‡§ and Brigitte Sallerin†‡§

*Université de Toulouse, CIRIMAT, UPS-INPT-CNRS, Faculté de Pharmacie, Toulouse, France
†INSERM, U858, Toulouse, France
‡Université de Toulouse, UPS, Faculté des Sciences Pharmaceutiques, Toulouse, France
§CHU Toulouse, Service de Pharmacie Hospitalière, Toulouse, France

Despite the success of alginate scaffolds and mesenchymal stem cells (MSCs) therapy in cardiac failure treatment, the impact of the physicochemical environment provided by alginate matrices on cell behavior has never been investigated. The purpose of this work was double: to determine the alginate composition influence on (1) encapsulated rat MSC viability, paracrine activity, and phenotype in vitro and (2) cardiac implantability and in vivo biocompatibility of patch shape scaffolds. Two alginates, differing in composition and thus presenting different mechanical properties when hydrogels, were characterized. In both cases, encapsulated MSC viability was maintained at around 75%, and their secretion characteristics were retained 28 days postencapsulation. In vivo study revealed a high cardiac compatibility of the tested alginates: cardiac parameters were maintained, and rats did not present any sign of infection. Moreover, explanted hydrogels appeared surrounded by a vascularized tissue. However, scaffold implantability was highly dependent on alginate composition. G-type alginate patches, presenting higher elastic and Young moduli than M-type alginate patches, showed a better implantation easiness and were the only ones that maintained their shape and morphology in vivo. As a consequence of alginate chemical composition and resulting hydrogel structuration, G-type alginate hydrogels appear to be more adapted for cardiac implantation.

Key words: Alginate; Cell encapsulation; Mesenchymal stem cells; Biomimetic materials; Heart

INTRODUCTION

The potential of mesenchymal stem cells (MSCs) for the treatment of myocardial infarction is now established. Their beneficial effects appear to be mainly attributed to their paracrine activities providing a regenerative microenvironment at the ischemic area (8,9,55,63). Direct injection in the necrotic zone of bone marrow (BM)-derived MSCs is already tested as a therapeutic strategy subsequently to myocardial infarction and reperfusion in clinical trials (62). Unfortunately, benefits of such regenerative therapy are limited by early cell death (around 85%) in the first 3 days after graft (34,38,48,54,57,61). These limitations depend on different mechanisms such as hypoxia, inflammation, or mechanical stress occurring during surgical implantation. Therefore, strategies concerning preservation of cell viability and functionality after implantation are becoming a priority in cardiac cell therapy (7,41,52,53). A promising strategy is to associate MSCs with a biocompatible material that (1) protects them during surgical intervention, (2) concentrates them on the ischemic area, (3) improves grafted MSC viability, (4) preserves their paracrine activities and their undifferentiated state, and (5) provides a physical support whose mechanical properties are in accordance with a cardiac implantation and in vivo environment.

Alginate hydrogels present an increasing interest to elaborate medical devices in cardiac therapy field. Different studies distinguished two main strategies using alginate-based biomaterials after myocardial infarction. The first one concerns injectable alginate implants as an acellular strategy (21,31,33,64,65). In this case, alginate is directly injected either into the myocardium or intracoronary to supply a physical support for improved healing and repair. The second strategy uses alginate hydrogels as cardiac patches for integration of newly formed vascularized tissue into the host myocardium (2,15,32). These examples validate the feasibility of using alginate as biomaterial in the treatment of heart diseases,

Received October 13, 2010; final acceptance October 28, 2011. Online prepub date: July 5, 2012.
Address correspondence to Caroline Ceccaldi, CIRIMAT, UPS-INPT-CNRS, Faculté de Pharmacie, 118 route de Narbonne, 31062 Toulouse Cedex 4, France. Tel: +33-5-62-25-68-37, Fax: +33-5-62-25-68-40; E-mail: ceccaldi@cict.fr

but little is known about the influence of alginate composition on biomaterial final properties in this domain.

Alginates are very hopeful for health applications due to their structural similarities with extracellular matrix, their properties to gelify under soft conditions and their low toxicity after purification. Alginates are a family of naturally derived polymers extracted from sea brown algae. Alginates are unbranched binary copolymers consisting of 1,4-linked β-D-mannuronic (M) and α-L-guluronic (G) residues organized in regions of sequential G units (G-blocks), regions of sequential M units (M-blocks), and regions of atactically organized G and M units. Sol–gel transition properties of alginates are based on the formation of a stiff "egg-box" structure due to the selective binding of divalent cations to G-blocks of two adjacent polymeric chains (18). As a consequence, the structure of alginate network is closely related to their monomeric and diadic organization. By varying their M/G proportions and distributions, it is possible to modulate the viscoelastic properties of the resulting crosslinked hydrogel.

In this context, it seems reasonable to hypothesize that the choice of the alginate composition may have a determining impact on the device characteristics and performance. Recent studies demonstrated the importance of cellular environment on matrix entrapped cells (16) and more particularly the effects of mechanical properties (5) and chemical composition (10,23,47,50,51,59) of alginates on stem cell behavior in pancreatic, neural, and cartilage tissue engineering fields. These observations underline the relevance of this parameter to design the best suitable device for the targeted application. Concerning cardiac applications, a complete bibliographic study reveals a lack of argumentation in this domain, as already reported injectable alginates and alginate patches appeared to be either G-type (2,15,21,31,33) or M-type (64,65), or even were sometimes not specified (1). As far as we know, the impact of alginate composition and resulting mechanical properties on MSC behavior has never been studied so far. With this scope, we firstly characterized two ultrapur alginate samples with similar molecular weight and different chemical compositions. Secondly, we compared the influence of alginate MSCs entrapment on cell viability and functionality in vitro. Finally, alginate composition influence was evaluated in vivo: calcium alginate hydrogels implantability and biocompatibility were evaluated after cardiac implantation in rats.

MATERIALS AND METHODS

MVG (G-type) and MVM (M-type) ultrapur grade sodium alginates were used (Provona up MVG and Provona up MVM, Novamatrix, Norway). Medium molecular weight alginates were chosen to improve mechanical properties of the materials and to limit their in vivo degradation (30).

Alginate Hydrogels Elaboration

Alginate concentration (1.2%, w/w) was chosen to optimize encapsulation process. Hydrogels were prepared under aseptic conditions (all solutions were sterile filtered and all equipment were autoclaved).

Alginate Dispersion. Solutions of 1.2% (w/w) MVG and MVM ultrapur alginate were prepared in iso-osmotic HEPES buffer (150 mM NaCl, 12.5 mM HEPES, pH 7.4) during 30 min at 1800–2000 rpm (Heidolph RZR-2041, Germany).

Hydrogels Gelification

In Vitro Study. MSCs were encapsulated in alginate microspheres, which permitted to study MSC behavior in alginate-confined environment. Microencapsulations were performed upon generation of monodisperse droplets of sodium alginate solution, containing MSCs (2.5 million of cells/ml of alginate solution) or not, by an encapsulator (IE50R, Inotech, Switzerland), equipped with a vibrating nozzle (300 μm, 850 Hz). Then ionotropic gelation was performed in an iso-osmotic buffer containing calcium ions ($CaCl_2$, 0.1 M) during 20 min. Constructs, containing approximately 2,300 cells per microsphere, were cultured in six-well plates in supplemented culture medium (α-MEM, 10% FBS, 1% penicillin/streptomycin, Gibco, France).

When necessary, cells were released from microspheres by incubation in 55 mM sodium citrate for 20 min to liquefy alginate. Cell suspension was then centrifuged (400 rpm, 5 min).

In Vivo Study. Alginate patches were elaborated to allow a very close contact between alginate-based materials and heart. Sodium alginate solutions were placed in 48-well plates. Then ionotropic gelation was performed in an iso-osmotic buffer containing calcium ions ($CaCl_2$, 0.1 M) for 20 min.

Alginate hydrogels were then washed three times (10 min in HEPES buffer) prior to in vitro cultivation or in vivo implantation.

^{1}H NMR Spectroscopy

Protocols used are derived from the method described by Grasdalen et al. (19). The ^{1}H NMR spectra of alginate in solution were recorded on a Avance DMX 500 MHz (Bruker Biospin Gmbh, Germany) operating at 500 MHz for ^{1}H using a 5-mm broadband inverse probe head (BBI 500 MHz). Prior to analysis, the average molecular weight of the alginate was reduced by a mild partial acid hydrolysis performed in two steps. Alginate (0.5 g) moistened with 5 ml ethanol (96%) was dissolved in 50 ml HCl (pH 1.5). The pH was adjusted to 5.0 by addition of NaOH

and hydrolyzed at 100°C under reflux for 10 min. After cooling to room temperature, the pH was adjusted to 3.0 by addition of HCl and heated at 100°C under reflux for 20 min. After cooling, the solution was neutralized (pH 7) by addition of NaOH and precipitated in ethanol (96%). The precipitate was left for drying overnight at 70°C. The hydrolyzed alginate was dissolved in D_2O (1.0%, w/v) and neutralized (pH 7), and 550 µl of the solution was filtered through a Whatman 13-mm syringe filter (pore size, 0.45 mm) into a 5-mm NMR tube. The spectra were recorded with a 90° pulse angle and a sweep width of 5,482 Hz. The acquisition time and recycle delay were both 2 s. Thirty-two scans were acquired, and the spectra were recorded with the same receiver gain. During acquisition, the sample temperature was 90°C. 3-(Trimethylsilyl)propionic acid-d4 sodium salt (TSP-d4) was used as chemical shift reference compound (d=0.0 ppm). The raw data were apodized by 1.0 Hz of exponential line broadening prior to Fourier transformation. No zero filling was applied.

Rheological Characterization

Rheological measurements were carried out using a stress-controlled rheometer (Rheostress RS75, HAAKE, Germany) with a parallel-plate geometry. Test samples were made to match the diameter of the parallel plate (20 mm). Gels were gently pressed with tissue paper to remove surface water before lowering the top plate. Stress sweeps at a constant frequency of 1 Hz were first performed to obtain the linear viscoelastic region for collecting subsequent data. Frequency sweeps were performed in the linear viscoelastic regime to determine the elastic (G') and viscous (G'') moduli values.

Texturometry

Young's moduli and mechanical behavior of microspheres were studied by three successive uniaxial compression assays (TA-XT2 Texture Analyzer, Stable Microsystems, UK). Briefly, mechanical resistance was determined as the main force required to generate a 50% compression of a sample of microparticles. The apparatus consisted of a mobile probe (314.16 mm^2) moving vertically up and down at constant and predefined velocity (0.5 mm/s). The force exerted by the probe on the microspheres was recorded as a function of the displacement, leading to a force versus strain curve. The results were expressed as the average maximal mechanical stress in kPa observed at 50% of strain from at least three independent observations.

Laser Diffraction Granulometry

Particles size distribution was assessed by laser diffraction granulometer (LS100, Coulter, US) on G-type and M-type alginate microparticles in iso-osmotic HEPES buffer. Sauter diameter $d(3,2)$ and polydispersity index were used to follow microspheres swelling, as an evaluation of microspheres stability over time.

Isolation and Culture of Rat MSCs

MSCs were obtained from BM of Lewis male rats (Harlan, France) weighing 180–200 g. Anesthesia was performed by intraperitoneal injection of pentobarbital (0.1 ml/100 g). BM was flushed from rat's femur with minimal essential medium (Gibco, France) supplemented with 10% fetal bovine serum (FBS) and 1% penicillin/streptomycin (Invitrogen, France) and centrifuged (400 × g, 5 min). Then cells were plated in culture flasks (100,000 cells/cm^2). After 3 days, nonadherent cells were removed by changing medium, and MSCs were recovered by their capacity to adhere highly to plastic culture dishes. MSCs were then routinely cultured and were used for the experiments. Most adherent cells expressed MSC markers CD90, CD29, CD106 and were negatives for CD34 (hematopoietic marker), CD45 (B cells marker), and CD31 (vascular cells marker). They were able to differentiate into cells from mesodermal lineage: osteoblasts, chondrocytes, and adipocytes. MSCs were used between the third and the sixth passage.

Quantification of Cell Viability

A live/dead assay was performed with viability/cytotoxicity kit (FluoProbes®, Interchim, France). Briefly, microspheres were washed two times with α-MEM/physiological serum (1:1) and immersed (30 min, 37°C) in presence of 2 µM ethidium homodimer-3 (necrotic marker measuring nucleus membrane integrity) and 1 µM calcein AM (viability marker measuring intracellular esterase activity) to stain dead cells in red and live cells in green. After washing with α-MEM, microspheres were observed by confocal microscopy (Zeiss LSM-FCS, Germany). Positive control for 100% cell death was obtained by treating microspheres containing encapsulated MSCs with 70% ethanol for 10 min prior to fluorescent live/dead staining.

Two parameters were measured. First, cell viability, V, was calculated as the percentage of viable entrapped cells. $V = N_L/(N_L + N_D)$ with N_L = Total green pixel number/number of green pixel per live cell and N_D = Total red pixel number/number of red pixel per dead cell. The second parameter was total cell density, D, expressed as the number of live and dead cells counted by microsphere area. $D = (N_L + N_D)/A_{\text{microsphere}}$ with $A_{\text{microsphere}}$ = area of the microsphere on which measurement was done.

Reverse Transcription-Polymerase Chain Reaction

Total RNA was isolated from 1 million of MSCs using RNeasy® Kit (Qiagen, France) according to the manufacturer's protocol. RNA (8 ng) was reverse transcripted to cDNA using the SuperScript II reverse transcriptase

(Invitrogen, USA). The real-time RT-PCR was performed using SYBR Green PCR Master Mix (ABI Prism 7000 HT Sequence Detection System, Applied Biosystems, USA). Amplification reactions (25 µl were carried out in triplicate with 5 µl of 1:10 diluted template cDNA) and the following primers (Eurogentec, Belgium) were used for the detection of vascular endothelial growth factor (VEGFα), hepatocyte growth factor (HGF), insulin-like growth factor (IGF1), epidermal growth factor (EGF), fibroblast growth factor (FGF2), and granulocyte colony-stimulating factor (G-CSF). Each assay was normalized by amplifying the housekeeping cDNA glyceraldehyde 3-phosphate dehydrogenase (GAPDH) and ribosomal protein L31 (RPL31) from the same cDNA sample and fold to nonencapsulated third passage MSCs.

VEGFα:	5′CAAAAACGAAAGCGCAAGAAA3′/ 5′GTCTGCGGATCTTGGACAAAC3′,
HGF:	AACAAGGTCTGGACTCACATG3′/ 5′CGTCTGGCTCCCAGAAGATATG3′,
IGF1:	5′GACGGGCATTGTGGATGAGT3′/ 5′GGATGGAACGAGCTGACTTTG3′,
EGF:	5′CTCACCCTCTCTCCTTGGAAAA3′/ 5′GGCGGGCATCCTGTGTT3′,
FGF2:	5′GTGTGTGCGAACCGGTACCT3′/ 5′TATTGGACTCCAGGCGTTCAA3′,
G-CSF:	5′TGTGGTGGTACCCAAGAAATCAC3′/ 5′CCTGGGCCCCTGAGACA3′,
GAPDH:	5′AGGTCGGTGTGAACGGATTTG3′/ 5′TGTAGACCATGTAGTTGAGGTCA3′,
RPL31:	5′CCATGGAGTGGGCTTCAAGA3′/ 5′TCTATGCGCACATCTGGAGTTC3′.

Western Blot

Proteins were extracted from MSCs using RIPA buffer. Analyses were performed with samples normalized for protein concentration. Membranes were probed with rabbit anti-FGF2 antibodies (1:500, Santa Cruz Biotechnology, USA). Following several washes in TBS-Tween (0.2%), membranes were incubated with horse radish peroxidase (HRP)-conjugated anti-rabbit secondary antibody (1:10,000, Santa Cruz Biotechnology, USA). Protein expression was normalized by GAPDH expression (1:1,000, Santa Cruz Biotechnology).

Differentiation Assays

Protocols used are derived from the methods of Neuhuber et al. (39).

Adipogenesis. MSCs were seeded into six-well plates at 20,000 cells/cm^2 and cultured until confluency. Cultures were placed in adipogenic induction medium (Dulbecco's modified Eagle's medium with 4.5 mg/ml glucose, 10% fetal bovine serum, 5% rabbit serum and antibiotics, with 0.5 mM isobutylmethylxanthine, 1 mM dexamethasone, 10 mg/ml insulin, and 1 mM indomethacin) for 3 days and subsequently moved to adipogenic maintenance medium (Dulbecco's modified Eagle's medium with 4.5 g/ml glucose, 10% fetal bovine serum, 5% rabbit serum, antibiotics, and 10 mg/ml insulin) for 1 day. After three cycles, cells remained in maintenance medium for 7 days prior to fixation with 4% paraformaldehyde. Cells were stained with Oil Red O to visualize neutral lipid accumulation.

Chondrogenesis. Five hundred thousand MSCs were pelleted in high-glucose Dulbecco's modified Eagle's medium with 1% fetal bovine serum, antibiotics, 50 mg/ml ascorbate 2-phosphate, 40 mg/ml proline, 2 mM pyruvate, insulin/transferrin/selenium/linoleic acid (ITSþ), 100 nM dexamethasone, 10 ng/ml transforming growth factor-b3, and 200 ng/ml recombinant bone morphogenic protein-2. Medium was changed three times per week. On day 21, pellets were fixed in 4% paraformaldehyde, embedded in paraffin, and sectioned (6 µm). Sections were stained with Alcian blue to reveal mucopolysaccharides and glycosaminoglycans.

Osteogenesis. MSCs were seeded in six-well dishes at 3,000 cells/cm^2. After 2 days, growth medium was replaced by osteogenic medium (including 100 nM dexamethasone, 50 mM ascorbate-2-phosphate, and 10 mM glycerol phosphate). All chemicals were purchased from Sigma-Aldrich, USA. Medium was replaced twice weekly. After 18 days, cells were stained with Alizarin Red S to visualize the calcify deposition.

In Vivo Implantation of Alginate Scaffolds

Experimental animals were handled in accordance with the European Animal Care Guidelines. Patch implantation was performed in adult female Sprague–Dawley rats (200–250 g) by left thoracotomy via the fourth intercostal space under general anesthesia (isoflurane, 2.5%) and mechanical ventilation. Alginate scaffolds ($n = 4$ for each alginate type) were implanted onto the surface of the left ventricle after removal of the pericardium over two peripheral sutures using a 7–0 prolene suture. Sham-operated animals were subjected to the same surgical procedure without implantation ($n = 2$).

Blood Analysis

Hematocrit measurement was performed on blood collected by retro-orbital bleeding on anesthetized animals using heparinized tubes. Hematocrits were evaluated by standard microhematocrit method. Leukocyte differential count was performed on total blood collected on abdominal aorta (MICROS-60, ABX-Diagnostics, France).

Echography

Left ventricular (LV) function was assessed in anesthetized animals with two-dimensional echocardiography with a General Electric Vivid 7® (GE Medical System, USA) equipped with a 13-MHz linear probe. For anesthesia, rats were induced with isoflurane and received continuous inhaled anesthetic (2%) for the duration of the imaging session. The animals were placed in the supine or lateral position on a warming pad. Numeric images of the heart were obtained in both parasternal long-axis and short-axis views. Two-dimensional end-diastolic and end-systolic long-axis views of the LV were standardized as follows: inclusion of the apex, the posterior papillary muscle, the mitral valve, and the aortic root. Two-dimensional echocardiographic measurements were performed with the cine-loop feature to retrospectively catch true end-diastolic and end-systolic phases, defined as the phases in which the largest and the smallest LV cavity sizes were obtained, respectively. End-diastolic and end-systolic areas (A) were obtained by hand tracings of the LV endocardial contours, according to the American Society of Echocardiography leading edge method. On these frames, end-diastolic and end-systolic lengths (L) of the LV were obtained by tracing a line connecting the more distal part of the apex and the center of a line connecting the mitral annular hinge points. End-diastolic and end-systolic volumes (LVEDVs and LVESVs, respectively) were then calculated by means of the single-plane area-length method ($\text{volume} = 8 \times A^2/3 \times \pi \times L$). LV ejection fraction (LVEF, %) was calculated as $[(\text{LVEDV} - \text{LVESV})/\text{LVEDV}] \times 100$. All measurements were averaged on three consecutive cardiac cycles and analyzed by a single observer who was blinded to the treatment status of the animals.

Cyto- and Histological Examinations

Staining of MSCs extracted from microspheres was performed after alginate solubilization and cell removal. Cells were plated in six-well plate, fixed in 4% paraformaldehyde, and stained with Alizarin Red S, Alcian Blue, or Oil Red O coloration using standard procedures. For cell staining in embedded microspheres, paraffin sections of G-type and M-type alginate microspheres were rehydrated and incubated in the presence of biotinylated rat proliferating cell nuclear antigen (PCNA) according to the manufacturer's recommendations. Sections were counterstained with hematoxylin. Sections of rat kidney regenerating after ischemia/reperfusion were used as positive control (29). For CD90 detection, paraffin sections of G-type and M-type alginate microspheres were rehydrated and incubated with anti-rat CD90 antibody (diluted 1:100, 60 min; Santa Cruz Biotechnology, CA). Antibody revelation was performed by using an Alexa Fluor 568 secondary antibody (1:500, 30 min; Invitrogen, CA). For nuclear detection, sections were incubated with to-pro-3 (1:1,000, 20 min; Invitrogen, CA). For histological staining on explanted hearts, hearts were collected and fixed in Carnoy's solution, and paraffin sections (6 μm) were rehydrated and stained with hematoxylin/eosin coloration using standard methods. α-Smooth muscle actin (α-SMA)-staining implanted heart sections were rehydrated and incubated with mouse monoclonal anti-α-SMA (clone 1A4, Sigma, USA) for 1 h. Tissue was stained using the anti-mouse HRP-DAB and counterstained with hematoxylin.

Statistical Analysis

Results are expressed as mean ± SD. Statistical comparison of the data was performed using the *t* test for comparison between two groups or one-way ANOVA and post hoc Tukey's test for comparison of more than two groups. A value of $p < 0.05$ was considered significant.

RESULTS

Characterization of Alginate Hydrogels

Determination of Diadic Composition of Alginates. Gelification process of alginate is described by the "egg-box" model where divalent cations are binded to regions enriched in G–G sequences to form intramolecular and/or intermolecular junctions. The ability of alginate to form a gel in presence of Ca^{2+} depends not only on its uronate composition but also on the repartition of mannuronic and guluronic residues along the polymeric chain (22). In this study, fraction of guluronic (F_G) and mannuronic (F_M) residues together with diadic composition (F_{GG}, F_{GM}, and F_{MM}) of ultrapur alginates were determined by ^{1}H-RMN spectroscopy. G-type alginate presented significantly more G residues and G–G sequences than M-type alginate (Table 1).

Mechanical Behavior of Alginate Hydrogels. Hydrogels synthesized with these two different alginates were then analyzed by measuring elastic modulus (G′) and loss modulus (G″) by oscillatory shear measurement in a rehometer. Whatever the frequency tested in their viscoelastic domain, both alginate types exhibited elastic moduli G′ higher than their loss moduli G″, confirming that both alginate types were under a hydrogel structured form at the calcium concentration tested for the experiments (0.1 M). As a consequence of its higher G fraction, G-type alginate calcium hydrogels presented higher moduli than M-type alginate hydrogels, revealing a higher structuration degree due to more calcium-binding sites (as can be seen in Table 1, for a frequency of 4 Hz). To complete calcium alginate hydrogels characterization, their mechanical properties were studied under compression strain. Young's modulus presents the advantage not

Table 1. Main Characteristics of Ultrapur Alginates Used in This Study

Parameters	Provona Up MVG	Provona Up MVM
F_G[a]	68%	45%
F_{GG}[a]	55%	28%
F_{GM}[a]	13%	17%
F_{MM}[a]	20%	38%
Elastic modulus (G′)[b]	31.1±2.6 kPa	9.9±2.7 kPa
Loss modulus (G″)[b]	4.2±0.6 kPa	1.3±0.5 kPa
Apparent viscosity[c] at 25°C, 1%	262 mPa.s	440 mPa.s
Protein content[c]	≤0.1%	≤0.1%
Endotoxins[c]	<19 EU/g	<25 EU/g

F_G, G fraction; F_{GG}, GG fraction; F_{GM}, GM fraction; F_{MM}, MM fraction.
[a]^{1}H NMR measurement.
[b]Rheological measurement at 4 Hz (mean ± standard deviation).
[c]Data provided by Nova Matrix, FMC BioPolymer (Oslo, Norway).

to be dependent of the device geometry but only of the intrinsic mechanical properties of the materials. The mechanical behavior of the two alginates was assessed by three successive compressions, and Young's modulus was determined at 50% of strain (Fig. 1). Alginate microspheres presented a Young's modulus near 38 and 25 kPa for G-type and M-type alginate, respectively. G-type alginate hydrogels showed a time-dependent mechanical resistance, which evidenced viscous or plastic behavior, while M-type alginate hydrogels maintained an elastic behavior over time.

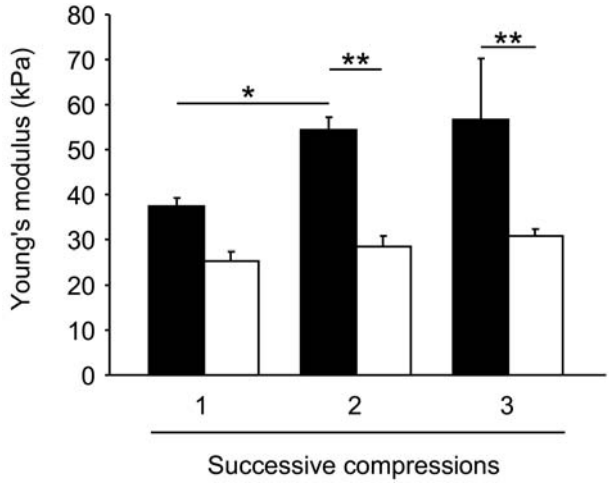

Figure 1. Mechanical properties of alginate hydrogels. Determination of Young's modulus of G-type (black bars) and M-type (white bars) alginate hydrogels by stress measurement under three successive 50% compressive strains (1, 2, and 3). Error bars represent standard deviation; *$p \leq 0.05$, **$p \leq 0.01$ based on ANOVA analysis.

Swelling Behavior of Alginate Hydrogels. Swelling behavior of alginate hydrogels is an essential parameter to describe the device stability in wet environment like during in vitro cultivation time or after animal implantation. Consequently, alginate microspheres were synthetized and immersed for 28 days in iso-osmotic buffer, and their Sauter diameter d(3,2) was weekly assessed by laser diffractometry (Fig. 2). Microspheres sizes and distribution remained stable during the entire immersion test and could consequently be considered as adapted for in vitro and in vivo studies, as no swelling, a sign of hydrogel destabilization, could be observed.

Immobilized MSC Biological Properties

Viability of Entrapped MSCs. Bone marrow MSC viability was assessed by confocal analysis. Encapsulated MSCs were cultured under proliferation conditions for 28 days, and viability of cells in G-type and M-type alginate microspheres was weekly determined. Cell viability was maintained around 80% (Fig. 3A) for 21 days after encapsulation; a slight decrease was observed from 28 days for both alginate types. Confocal *z* planes (Fig. 3B and C) of microspheres at 21 days postencapsulation showed a homogenous distribution of viable cells in whole microspheres.

Cell density *D* was estimated at 151±7.8 and 167±25.2 MSCs/mm^2 for G-type and M-type alginate microspheres, respectively (mean±SD; $p>0.05$) and was found to remain stable along the study. Furthermore, MSC-encapsulated in G- and M-type microspheres did not exhibit any proliferation. Indeed, as observed in Figure 4A–D, G-type and M-type alginate microsphere sections did not show PCNA immunostaining at day 28 postencapsulation. This observation, combined

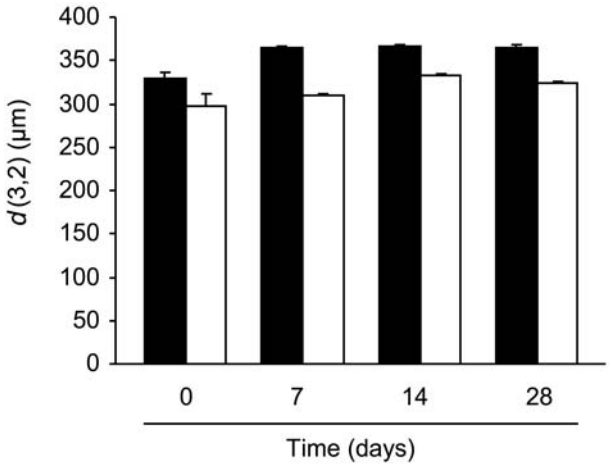

Figure 2. Swelling behavior of alginate hydrogels. Sauter diameter *d*(3,2) of G-type (black bars) and M-type (white bars) alginate microspheres immersed for 28 days in iso-osmotic buffer.

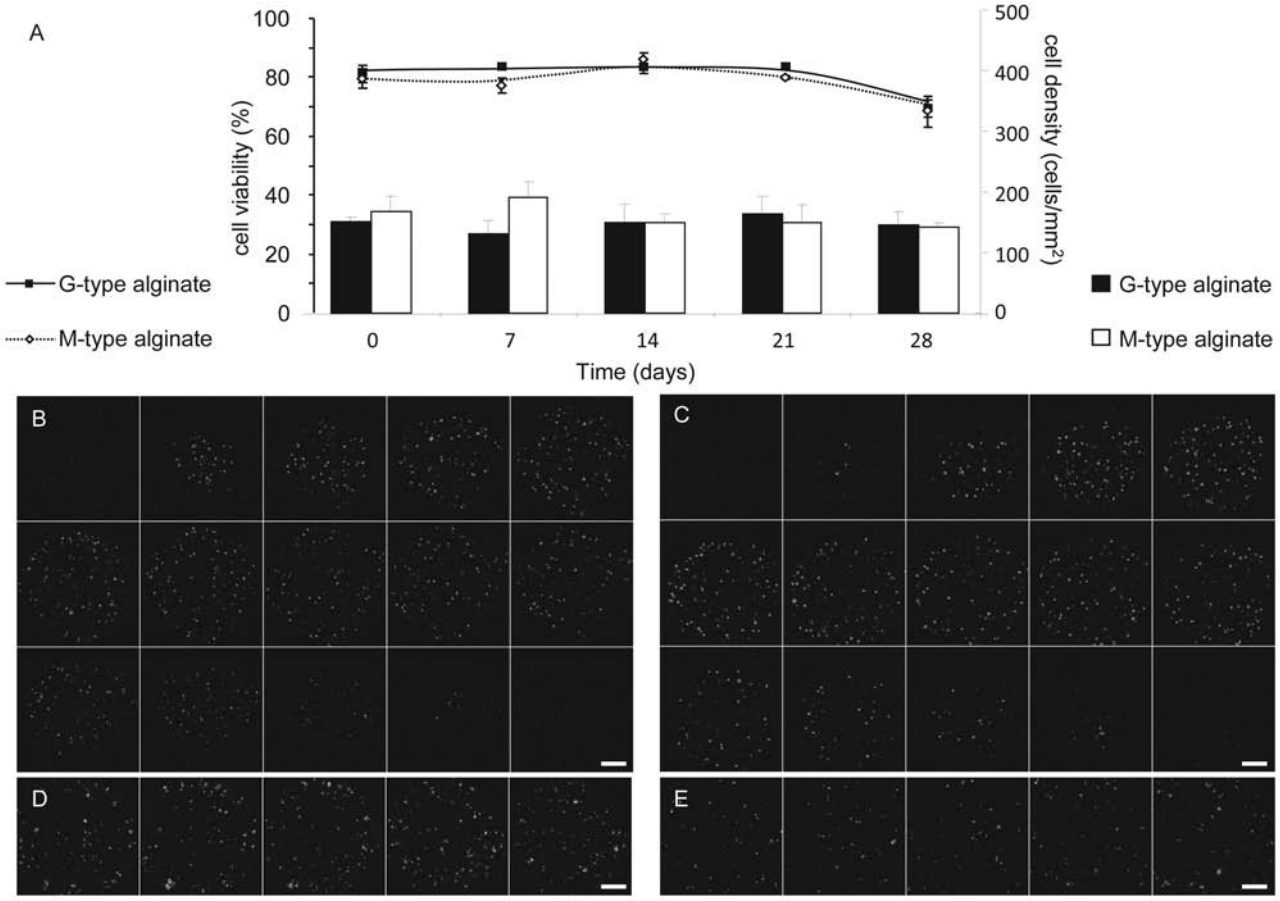

Figure 3. Viability of entrapped MSCs in alginate hydrogels. Quantification of mesenchymal stem cell (MSC) viability (%) and alginate cell density (cells/mm^2) by confocal microscopy during 28 days of encapsulation in G-type (full line/black bars, respectively) or M-type (dot line/white bar, respectively) alginate microspheres (A). Confocal *z* planes of G-type (B) and M-type (C) alginate microspheres after a live/dead staining after 21 days in culture. Five confocal *z* planes of G-type (D) and M-type (E) alginate microspheres after ethanol treatment showing a diffuse labeling of dead cells with some residual living cells. Scale bars: 200 μm.

with the absence of significant variation in cell density inside microspheres during culture time, suggests that encapsulated MSCs do not underlie proliferation. This may be related to an alginate/MSC contact inhibition due to the highly confined alginate microenvironment (26,45). These results suggest neither proliferation of MSCs in alginate microspheres nor MSCs decrease over time.

Functionality of Entrapped MSCs. Next we investigated whether encapsulation may affect MSC phenotype. As a first approach, we demonstrated that, after 28 days of encapsulation, 84% ± 3.76% and 86% ± 4.5% of the total cell population for G-type and M-type alginates, respectively (mean ± SD; percentage determined by peroxidase revelation, $p > 0.05$), were positive for the MSC marker CD90. Then we investigated whether encapsulated MSCs undergo spontaneous differentiation toward classical mesodermal lineage. With this scope, we stained MSCs extracted from G-type or M-type alginate after 28 days with Alizarin red S, Alcian Blue, and Red Oil O specific dyes for osteogenic, chondrogenic, and adipogenic lineage. As shown in Figure 5, in contrast to control MSCs in which specific lineage was chemically induced in vitro, MSCs eluted from microsphere were not stained by any of these dyes. This indicates that encapsulation into G-type and M-type alginate did not induce the commitment of MSCs toward mesodermal lineage.

We have previously shown that paracrine factors, playing a major role in the beneficial effect of cell therapy, were secreted by MSCs (36). As shown in Figure 6A, we found that expressions of cytokines normally produced by MSCs (VEGF, IGF-1, FGF2, HGF, EGF, and G-CSF) were increased for both alginate types as compared to nonencapsulated cells. In addition, the amount of intracellular FGF2, quantified by Western blot, was not modified after MSC encapsulation (Fig. 6B).

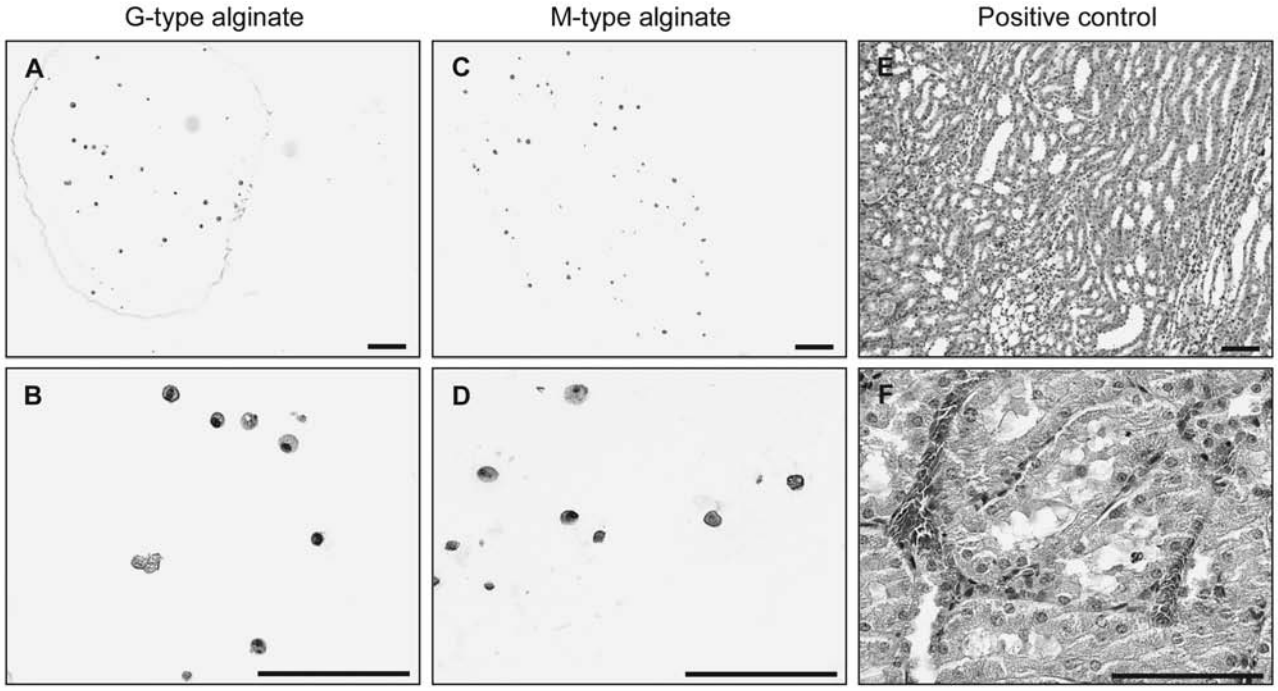

Figure 4. PCNA immunostaining of encapsulated MSCs. Proliferating cell nuclear antigen (PCNA)-immunostained G-type (A and B) and M-type (C and D) microspheres after 28 days postencapsulation. Sections of rat kidney regenerating after ischemia/reperfusion were used as positive control (E and F). Scale bars: 100 μm.

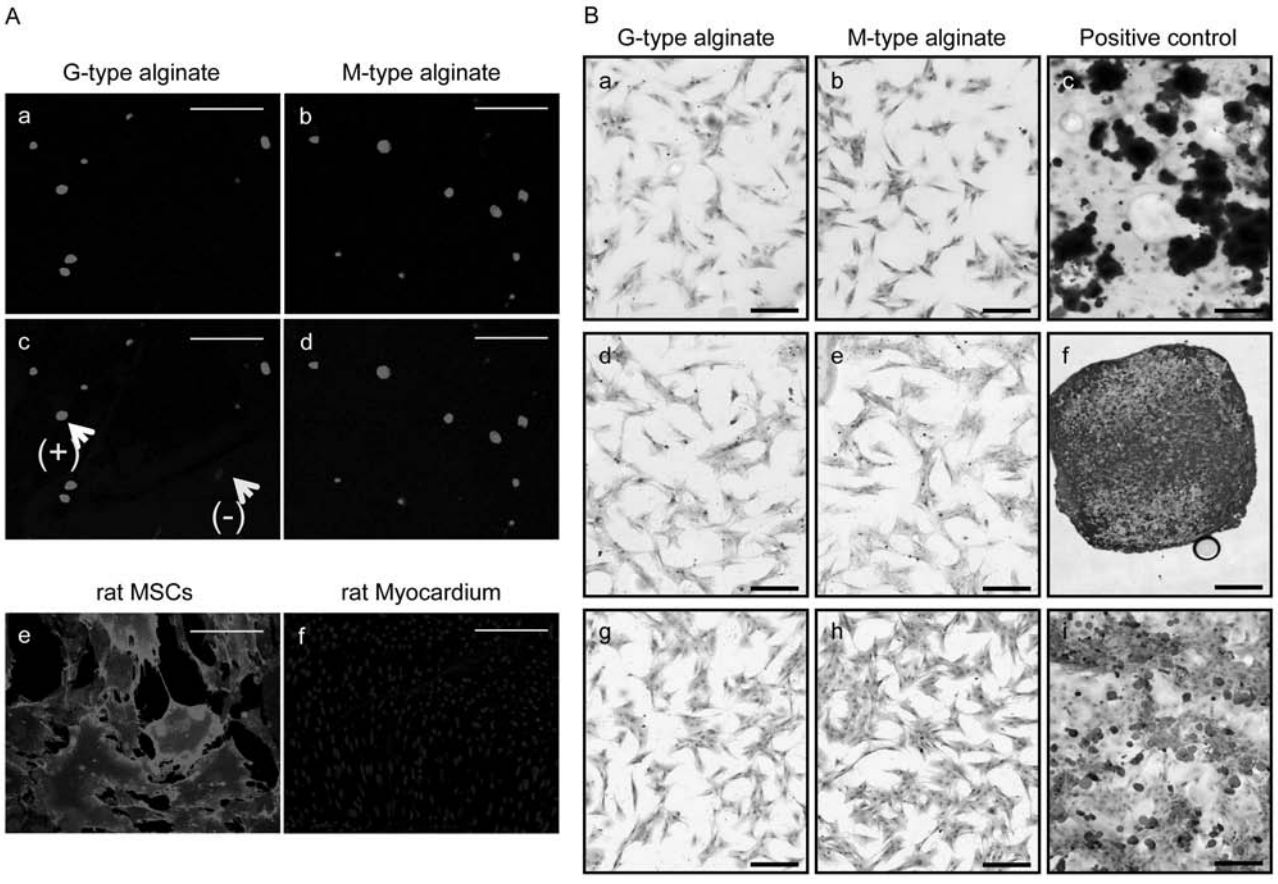

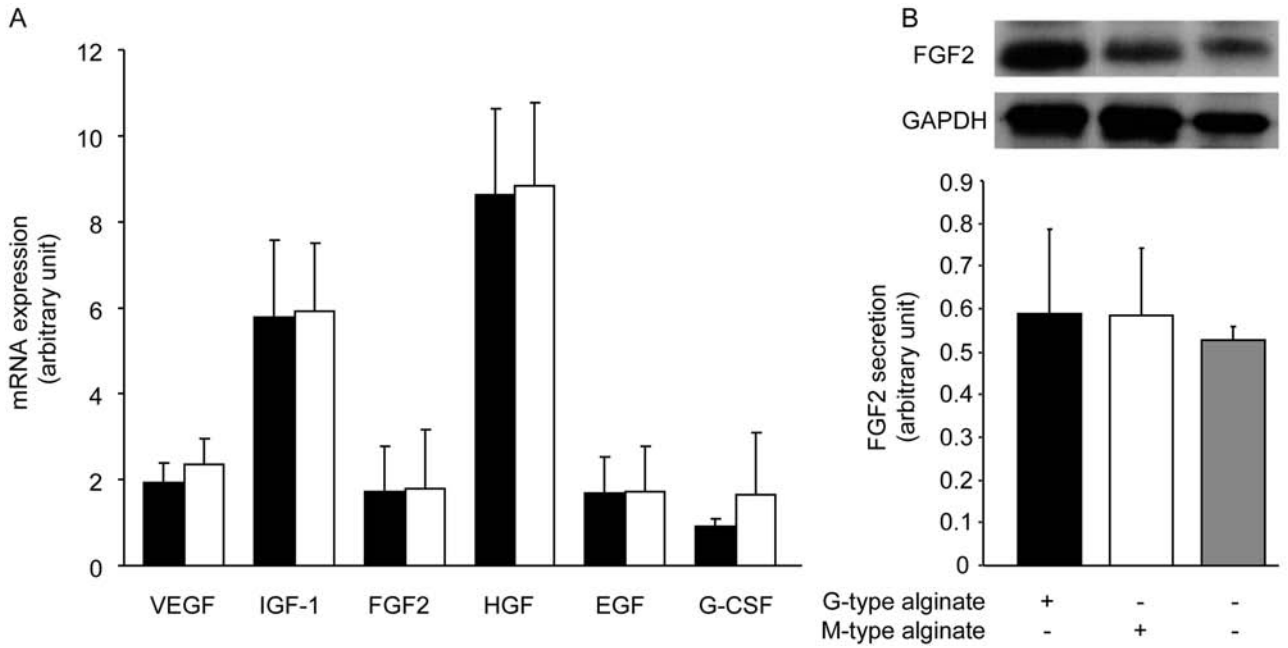

Figure 6. Paracrine activity of encapsulated MSCs. Relative quantification of transcript coding for growth factors in MSCs encapsulated in G-type (black bars) or M-type (white bars) alginate microspheres after 28 days of culture, normalized by glyceraldehyde 3-phosphate dehydrogenase (GAPDH) and ribosomal protein L31 (RPL31), fold to control (A). Control is determined by cytokine expression in cultured MSCs. Quantification of intracellular fibroblast growth factor 2 (FGF2) in MSCs encapsulated in G-type (black bars) or M-type (white bars) alginates microspheres after 28 days of culture or nonencapsulated MSCs (gray bars) normalized by GAPDH (B).

In Vivo Alginate Scaffolds Cardiac Compatibility

Implantability of Alginate Scaffolds. Alginate scaffolds were implanted and fixed to the myocardium by two peripheral sutures. All were successfully attached. However, M-type alginate scaffolds appeared to be more difficult to manipulate during surgical intervention due to their friability and their poor mechanical properties.

Cardiac Biocompatibility of Alginate Scaffolds. The effect of alginate scaffolds implantation on adult rat heart was studied. Hematocrits were weekly analyzed (Fig. 7A) during implantation time, and white blood cells (Fig. 7B) were numbered after 28 days postimplantation. No significant differences were observed for these parameters between control group, G-type and M-type alginate implanted groups, suggesting that rats did not present any sign of systemic infection or inflammation.

Cardiac function was weekly determined by echocardiography after implantation. Left ventricular end-diastolic volumes (LVEDV; Fig. 8D), ejection fraction (EF; Fig. 8E), and heart rate (HR; Fig. 8F) showed no significant change in comparison with nonimplanted rat and were stable for 1 month.

Macroscopic and Microscopic Observations of Explants. Postmortem analyses after 28 days postimplantation revealed that no adherences were observed in the environment of implanted scaffolds. G-type alginate scaffolds were found still attached to the myocardium, conserving their initial morphology (Fig. 9A). On the contrary, M-type alginate scaffolds were found detached from suture, near the heart, in thoracic wall. They were no longer in a patch shape (Fig. 9B).

Eosin/hematoxylin staining of implanted heart revealed normal myocardium (Fig. 10A and B) with foreign body

FACING PAGE

Figure 5. CD90 detection and differentiation staining of entrapped MSCs. (A) Confocal microscopy observations of CD90 alone (a, b) or overlay (c, d) of CD90 and cell nuclei of entrapped MSCs in G-type (a, c) and M-type (b, d) at 28 days postencapsulation. (−) and (+) labeled arrows show CD90-negative MSC and CD90-positive MSC, respectively. (e and f) Overlays of positive (rat MSCs) and negative controls (rat myocardium), respectively. Scale bars: 100 μm. (B) Specific coloration of osteogenic (Alizarin Red: a, b, and c), chondrogenic (Alcian Blue: d, e, and f), and adipogenic lineage (Red Oil: g, h, and i) of MSCs: optical microscopy of 28 days postencapsulated MSCs in G-type (a, d, and g) or M-type alginate hydrogels (b, e, and h). Positive controls: MSCs after induction of osteogenesis (c), chondrogenesis (f), and adipogenesis (i). Scale bars: 200 μm.

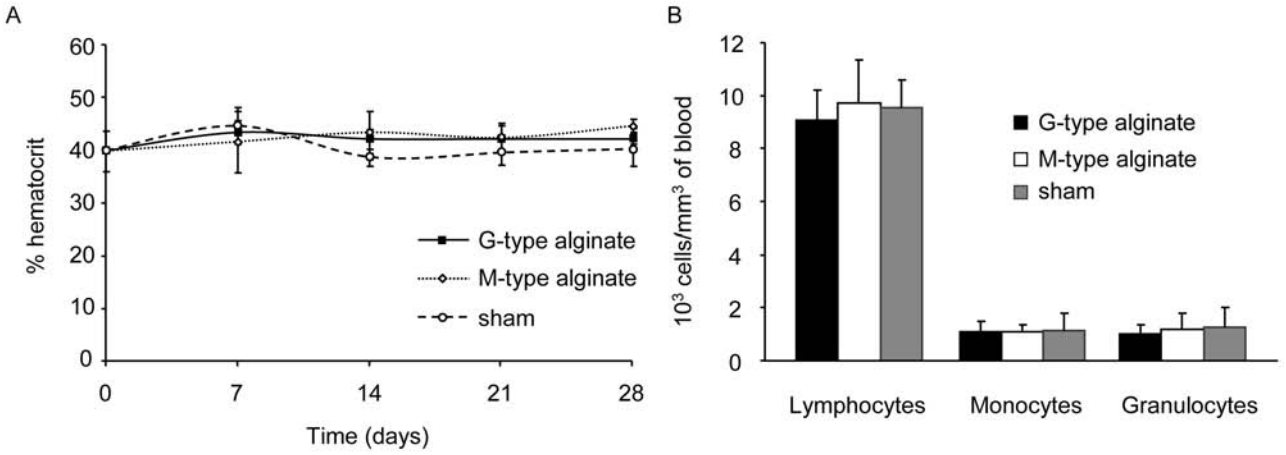

Figure 7. Evaluation of alginate hydrogels biocompatibility. Hematocrit levels of implanted rats 28 days after cardiac implantation (A) of G-type (full line), M-type (dot line) hydrogels and control group (dash line). White blood cell differential count 28 days after cardiac implantation (C) of G-type (black bars) and M-type (white bars) alginate scaffolds implanted group and control group (gray bar).

giant cells and macrophages at the alginate/myocardium interface. This histomorphological feature is compatible with a classical foreign body reaction probably related to alginate hydrogels. A weak fibrosis surrounding scaffolds was associated with the formation of neovascularization as indicated by arrows in Figure 10C. In the case of M-type alginate, the presence of fibers and cells infiltrating scaffolds was also observed (Fig. 10D). The granulation tissue surrounding scaffolds formed a fibrous capsule. All together, these histomorphological features indicate that implantation of alginate microspheres induced a classical local inflammatory response, as previously reported by other groups (3,35,44).

DISCUSSION

Despite the success of alginate scaffolds and mesenchymal stem cells therapy in cardiac failure treatment, the impact of the physicochemical environment provided by alginate matrices on cell behavior has never been investigated in this application. The purpose of this work was double, to determine alginate composition influence on (1) encapsulated MSC viability, paracrine activity, and phenotype in vitro and (2) cardiac implantability and in vivo biocompatibility of patch shape scaffolds.

In this study, two different alginates, both exhibiting a medium molecular weight, have been selected upon their M/G ratio: a low M/G ratio alginate, so-called G-type alginate, and a high M/G ratio alginate, so-called M-type alginate. NMR characterization showed that selected samples exhibit a G fraction of 68% and 45% and a G-blocks fraction of 55% and 28%, respectively. Shear measurement and determination of swelling behavior revealed that calcium crosslinking of 1.2% G-type and M-type alginate permitted in both cases to obtain a structured and stable polymeric network corresponding to a hydrogel. Characterization of these calcium alginate hydrogels showed that the M/G ratio impacted not only the matrices mechanical strength but also their mechanical behavior: G-type hydrogels were more rigid and presented viscous and/or plastic behavior; on the contrary, M-type hydrogels were less rigid and exhibited an elastic behavior. These macroscopic observations can be explained by differences in chemical compositions and structure of the tested alginates. Effectively, their sol–gel transition involves an "egg-box" model (18) through the ionic interaction between divalent cations, in our case, Ca^{2+} ions, and adjacent guluronic residues of alginate chain. Therefore, when decreasing M/G ratio and increasing G-blocks content, a denser polymeric network can be obtained (22), leading to a more rigid scaffold, less able to swell after compression (40). These latter properties could explain the viscous and/or plastic mechanical behavior observed in the case of G-type hydrogels. Mechanical properties of G-type and M-type alginate hydrogels were statistically different, but both remained compatible with cardiac implantation, as their mechanical strengths match with myocardium tissue Young's modulus; their levels of elasticity seem to be in accordance with dynamical heart environment (66). Concerning MSCs, recent studies demonstrated that the mechanical properties of cell environment (provided by the biomaterial) can have a notifying impact on their behavior. Engler et al. (16) cultivated MSCs on polyacrylamide gels with varying Young's moduli corresponding to the mechanical properties of various organs. They reported that MSCs committed the lineage specified by matrix elasticity, predominantly to the lineage expected after specific cytokine induction. This influence of microenvironment chemical and physical properties was also observed on

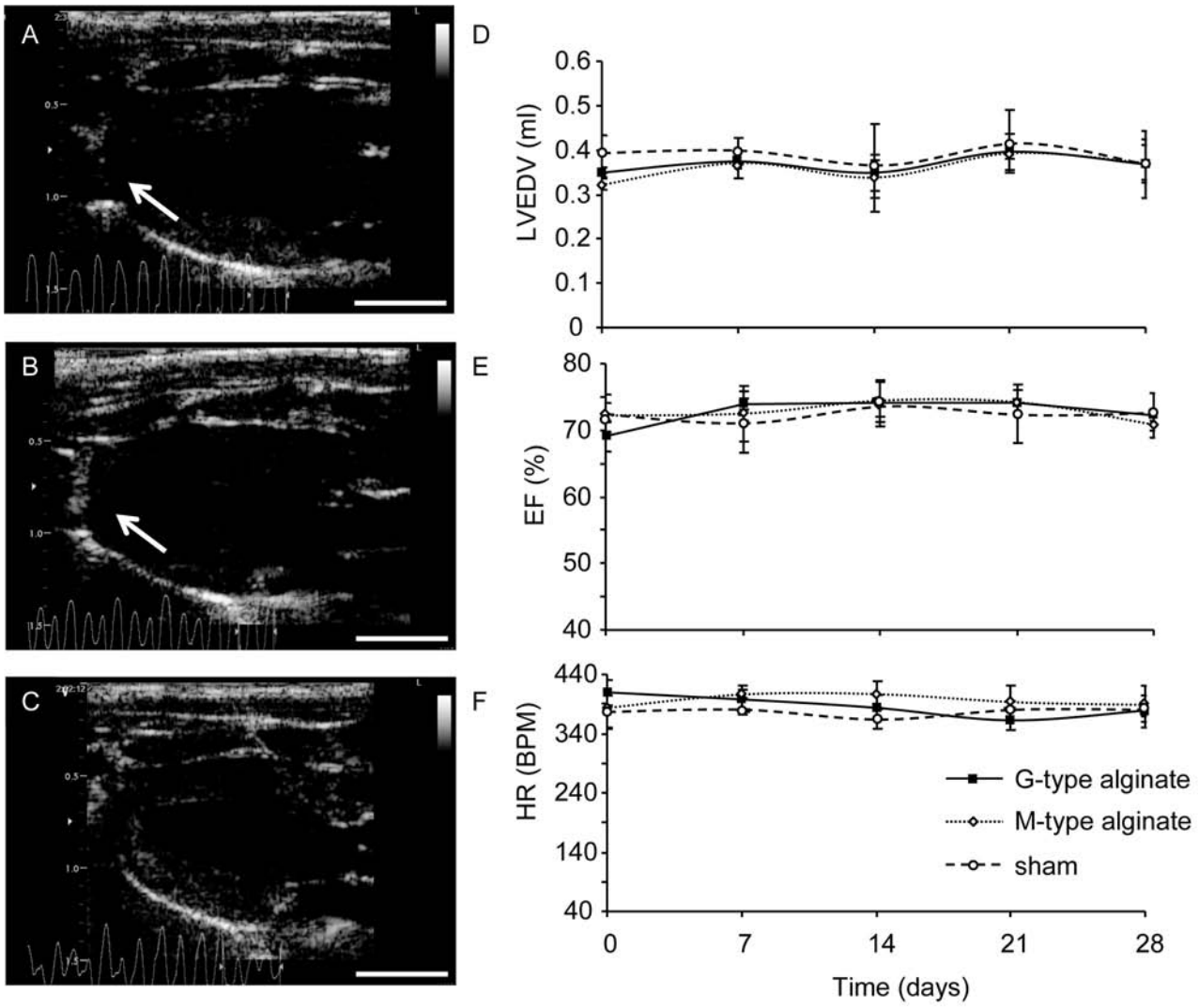

Figure 8. Results of echographic measurement. Left: Echographic photography of implanted (A and B) and not implanted (C) hearts. G-type (A) and M-type (B) alginate scaffolds are indicated by arrows. For understanding facility scale bars corresponding to 5 mm have been added. Right: Left ventricular end-diastolic volumes (LVEDV, D), left ventricular ejection fraction (LVEF, E), and heart rate (HR, F) in beats per minute (BPM) of G-type (full line) and M-type (spot line) alginate scaffolds implanted rats and controls (dash line) 28 days after cardiac implantation.

cells embedded in alginate hydrogels for diabetes therapy purpose. Alginate M/G ratio modulated entrapped murine insulinoma βTC3 cells functionality (10,23,50,51). Such phenomenon was also reported in the case of stem cells. It has been demonstrated that providing to neural stem cells an alginate environment whose mechanical properties are close to those of brain tissues can upregulate neural markers and modify their paracrine activities when varying alginate M/G ratio (5,47). Hence, the choice of alginate composition when elaborating a scaffold, a fortiori in a cardiac application where scaffold mechanical behavior appears as a critical parameter, is far from neutral. Surprisingly, it has never been studied till then.

In this study, in vitro evaluation of G-type and M-type alginates confirmed that both hydrogels were good candidates for MSC encapsulation. MSC viability was maintained around 75% up to 28 days postencapsulation. Moreover, live/dead cells distribution inside microspheres suggested sufficient nutriments and oxygen diffusion in whole microparticles, a necessary prerequisite to maintain cell viability (37).

Functionality of encapsulated MSCs was evaluated through the expression of cytokines responsible of MSCs' beneficial effects. Bioactive factors secreted by MSCs possess angiogenic, antiapoptotic, and immunomodulatory properties that may limit tissue damage

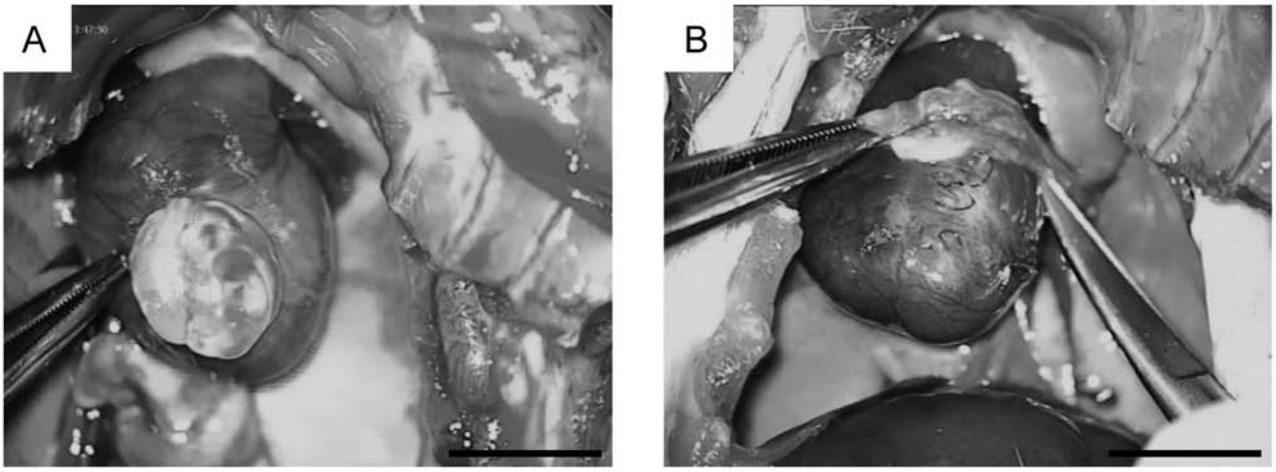

Figure 9. Macroscopic morphology of explanted alginate hydrogels. Photography of G-type (A) and M-type (B) alginate scaffolds explanted from the heart 28 days after implantation. Scale bars: 10 mm.

extension at the injury site and promote blood supply (9,12,17,25). Among them, FGF-2, HGF, VEGF, G-CSF, EGF, and IGF-1 were clearly identified in literature (4,13,14,20,24,49,56), FGF-2 being the most abundant cytokine secreted by MSCs (36). The measurement of mRNA encoding for these factors and the quantification of intracellular FGF2 showed that MSC paracrine activity was maintained and even increased when encapsulated. Statistical analysis concerning the comparison of biofactor expression levels in encapsulated and nonencapsulated MSCs showed an overexpression of IGF-1 and HGF in the former case ($p<0.001$). It has already been demonstrated that three-dimensional configuration can modify biofactor expression levels in encapsulated cells (11). Such mechanisms seem to be related to changes (i) in spatial and mechanical configuration mimicking in vivo environment and (ii) in cell morphology, movement, and density (16,28,51,60).

Concerning cell phenotype, our results showed that most of the entrapped cells express the MSC marker CD90 and maintain the osteogenic, chondrogenic, and adipogenic lineage. These results confirm that most of the entrapped cells maintain the MSC phenotype. MSCs did not undergo transdifferentiation to classical osteoblast, chondroblast, and adipocyte lineages during culture period and expressed the MSC marker CD90, confirming that entrapped cells maintain an MSC phenotype.

Regarding MSC biological parameters investigated here, alginate M/G ratio had no direct impact on their behavior after 28 days of encapsulation. These results confirmed previous work from our laboratory, which demonstrated that encapsulation in alginate microparticles represents a promising approach for MSC engraftment on solid organ (58). Our in vitro results suggest that entrapment in three-dimensional scaffolds elaborated with both types of alginates may represent an excellent alternative to direct intraparenchymal injection and could permit to take advantage of paracrine properties of MSCs in cell therapy. Nevertheless, this conclusion has to be modulated by our in vivo results.

Implanted rats presented no sign of infection and a stable cardiac function, suggesting a good environmental and mechanical compatibility of the devices on beating heart. Patch-shaped scaffolds from G-type and M-type alginate did not disturb cardiac function when implanted on the myocardium. Alginates biocompatibility in relation with their composition and more particularly with their M/G ratio has been a matter of controversy (27,43,44). Consensus is now established about the predominant influence of purity grade on alginate immunogenicity (42,46). This point was confirmed by the observed maintained hematocrit level in both cases during the implantation period. In addition, both alginate scaffolds were well integrated in the myocardial environment: microscopic observation of explants revealed a weak fibrosis associated with a vascularized tissue surrounding the devices. This latter observation is of importance, as oxygenation and nutrition of entrapped cells is a key parameter to obtain long-term viability of the graft, a point that actually limits the benefits of MSC cardiac therapy. Concerning cardiac implantability, two distinct in vivo behaviors were observed as a function of alginate M/G ratio. M-type alginate scaffolds have been more difficult to manipulate due to their lack of cohesion and lower rigidity when compared to G-type alginate scaffolds. These latter were easily manipulated by surgeon and fixed by suture to the myocardium. Twenty-eight days postimplantation, G-type scaffolds

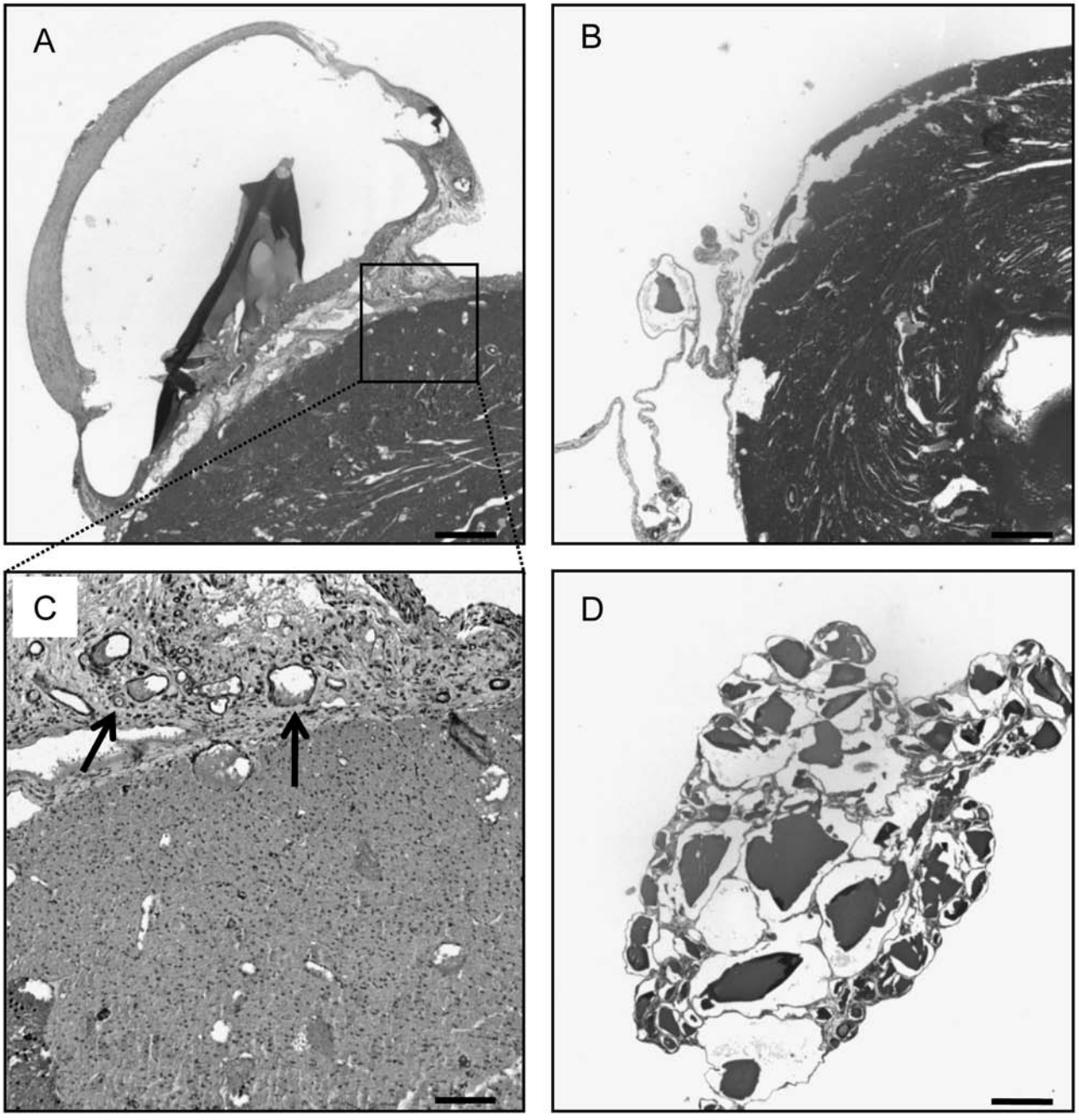

Figure 10. Twenty-eight days postimplantation microscopic analysis of explanted alginate hydrogels from the heart. Eosin/hematoxylin staining of explanted G-type (A) and M-type (B and D) alginate scaffolds. α-SMA staining of explanted G-type alginate hydrogel (C); arrows indicate vascular formation in fibrotic tissue. Scale bars: 500 μm (A, B, and D) and 100 μm (C).

were found on the myocardium, still fixed by the initial sutures, while M-type alginate scaffolds were found damaged and detached from sutures. Alginate degradability is generally reported to depend on molecular weight (6). In this study, G-type and M-type alginate viscosities were similar (262 and 440 mPa s, respectively; Table 1), suggesting the same order of magnitude of their molecular weight. Hence, the observed M-type alginate patch destruction may be better related to hydrogel microstructure and resulting mechanical properties. Effectively, G-type alginates, containing a higher F_{GG} fraction than M-type alginates, provide more binding sites for calcium ions, leading to more structured and rigid polymeric networks. Consequently, G-type alginate

scaffolds were able to support strain in a dynamic environment, while less structured M-type alginate scaffolds could not.

CONCLUSION

This study presents a double interest: first, it validates the use of alginate three-dimensional scaffolds to take advantage of MSCs' secretory abilities. Second, it points out the impact of alginates chemical composition and, consequently, mechanical behavior on scaffold performance in cardiac therapy field. Even if both alginate types appear highly biocompatible, resulting scaffold implantability and in situ mechanical resistance are to be considered. Alginate G-type hydrogels, exhibiting a higher structural and mechanical resistance, appeared better adapted to bear in vivo cardiac strain.

This study permits expanded knowledge of the critical parameters to consider when considering an alginate MSC scaffold. However, many questions remain unsolved, particularly concerning the device optimal tridimensional geometry. Recent studies have highlighted the interest of a patch shape, but little is known concerning the optimal porosity necessary to combine efficient cell loading, adequate mechanical properties, nutrients circulation, and vascular infiltration. Strategies to optimize alginates scaffold performance for MSC cardiac therapy are currently under investigation in our laboratory.

ACKNOWLEDGMENTS: We wish to acknowledge H. Ternet for assistance for alginate hydrolysis (Université de Toulouse, CIRIMAT, UPS-INPT-CNRS, Faculté de Pharmacie, Toulouse). We thank A. Milon and O. Saurel at IPBS for providing access to NMR spectrometer (Réseau RMN, Midi-Pyrénées). We wish to acknowledge P. Ramos for his assistance in NMR measurement and process. We are grateful for the excellent technical support and advice of B. Payré and R. d'Angelo (Cellular Imaging Facility, IFR150-Rangueil, TRI Plateform, Toulouse). We thank S. Estage and A. Estival for assistance in tissue embedding and processing (Service d'anatomie et cytology pathologiques, CHU Rangueil, Toulouse) and C. Frugier (INSERM, U858, Toulouse, F-31432 France) for histological analysis. This work was supported by CNRS (CNRS grant for exploratory projects "Interface Matériau/Vivant"). The authors declare no conflicts of interest.

REFERENCES

1. Al Kindi, A. H.; Asenjo, J. F.; Ge, Y.; Chen, G. Y.; Bhathena, J.; Chiu, R. C.; Prakash, S.; Shum-Tim, D. Microencapsulation to reduce mechanical loss of microspheres: Implications in myocardial cell therapy. Eur. J. Cardiothorac. Surg. 39(2):241–247; 2010.
2. Amir, G.; Miller, L.; Shachar, M.; Feinberg, M. S.; Holbova, R.; Cohen, S.; Leor, J. Evaluation of a peritoneal-generated cardiac patch in a rat model of heterotopic heart transplantation. Cell Transplant. 18(3):275–282; 2009.
3. Anderson, J. M.; Rodriguez, A.; Chang, D. T. Foreign body reaction to biomaterials. Semin. Immunol. 20(2):86–100; 2008.
4. Angoulvant, D.; Ivanes, F.; Ferrera, R.; Matthews, P. G.; Nataf, S.; Ovize, M. Mesenchymal stem cell conditioned media attenuates in vitro and ex vivo myocardial reperfusion injury. J. Heart Lung Transplant. 30(1):95–102; 2011.
5. Banerjee, A.; Arha, M.; Choudhary, S.; Ashton, R. S.; Bhatia, S. R.; Schaffer, D. V.; Kane, R. S. The influence of hydrogel modulus on the proliferation and differentiation of encapsulated neural stem cells. Biomaterials 30(27):4695–4699; 2009.
6. Boontheekul, T.; Kong, H. J.; Mooney, D. J. Controlling alginate gel degradation utilizing partial oxidation and bimodal molecular weight distribution. Biomaterials 26(15):2455–2465; 2005.
7. Bursac, N. Cardiac tissue engineering using stem cells. IEEE Eng. Med. Biol. Mag. 28(2):80, 82, 84–86, 88–89; 2009.
8. Caplan, A. I. Adult mesenchymal stem cells for tissue engineering versus regenerative medicine. J. Cell. Physiol. 213(2):341–347; 2007.
9. Caplan, A. I.; Dennis, J. E. Mesenchymal stem cells as trophic mediators. J. Cell. Biochem. 98(5):1076–1084; 2006.
10. Constantinidis, I.; Rask, I.; Long, R. C., Jr.; Sambanis, A. Effects of alginate composition on the metabolic, secretory, and growth characteristics of entrapped beta TC3 mouse insulinoma cells. Biomaterials 20(21):2019–2027; 1999.
11. Dado, D.; Levenberg, S. Cell-scaffold mechanical interplay within engineered tissue. Semin. Cell. Dev. Biol. 20(6):656–664; 2009.
12. da Silva Meirelles, L.; Caplan, A. I.; Nardi, N. B. In search of the in vivo identity of mesenchymal stem cells. Stem Cells 26(9):2287–2299; 2008.
13. Delgaudine, M.; Lambermont, B.; Lancellotti, P.; Roelants, V.; Walrand, S.; Vanoverschelde, J. L.; Pierard, L.; Gothot, A.; Beguin, Y. Effects of granulocyte-colony-stimulating factor on progenitor cell mobilization and heart perfusion and function in normal mice. Cytotherapy 13(2):237–247; 2011.
14. Di Nicola, M.; Carlo-Stella, C.; Magni, M.; Milanesi, M.; Longoni, P. D.; Matteucci, P.; Grisanti, S.; Gianni, A. M. Human bone marrow stromal cells suppress T-lymphocyte proliferation induced by cellular or nonspecific mitogenic stimuli. Blood 99(10):3838–3843; 2002.
15. Dvir, T.; Kedem, A.; Ruvinov, E.; Levy, O.; Freeman, I.; Landa, N.; Holbova, R.; Feinberg, M. S.; Dror, S.; Etzion, Y.; Leor, J.; Cohen, S. Prevascularization of cardiac patch on the omentum improves its therapeutic outcome. Proc. Natl. Acad. Sci. USA 106(35):14990–14995; 2009.
16. Engler, A. J.; Sen, S.; Sweeney, H. L.; Discher, D. E. Matrix elasticity directs stem cell lineage specification. Cell 126(4):677–689; 2006.
17. Gnecchi, M.; He, H.; Liang, O. D.; Melo, L. G.; Morello, F.; Mu, H.; Noiseux, N.; Zhang, L.; Pratt, R. E.; Ingwall, J. S.; Dzau, V. J. Paracrine action accounts for marked protection of ischemic heart by Akt-modified mesenchymal stem cells. Nat. Med. 11(4):367–368; 2005.
18. Grant, G. T.; Morris, E. R.; Rees, D. A.; Smith, P. J. C.; Thom, D. Biological interactions between polysaccharides and divalent cations: The egg-box model. FEBS Lett. 32(1):195–198; 1973.
19. Grasdalen, H.; Larsen, B.; Smidsrød, O. A p.m.r. study of the composition and sequence of uronate residues in alginates. Carbohydr. Res. 68(1):23–31; 1979.
20. Guo, Y. H.; He, J. G.; Wu, J. L.; Yang, L.; Zhang, D. S.; Tan, X. Y.; Qi, R. D. Hepatocyte growth factor and granulocyte colony-stimulating factor form a combined

neovasculogenic therapy for ischemic cardiomyopathy. Cytotherapy 10(8):857–867; 2008.
21. Hao, X.; Silva, E. A.; Mansson-Broberg, A.; Grinnemo, K. H.; Siddiqui, A. J.; Dellgren, G.; Wardell, E.; Brodin, L. A.; Mooney, D. J.; Sylven, C. Angiogenic effects of sequential release of VEGF-A165 and PDGF-BB with alginate hydrogels after myocardial infarction. Cardiovasc. Res. 75(1):178–185; 2007.
22. Jorgensen, T. E.; Sletmoen, M.; Draget, K. I.; Stokke, B. T. Influence of oligoguluronates on alginate gelation, kinetics, and polymer organization. Biomacromolecules 8(8):2388–2397; 2007.
23. King, A.; Lau, J.; Nordin, A.; Sandler, S.; Andersson, A. The effect of capsule composition in the reversal of hyperglycemia in diabetic mice transplanted with microencapsulated allogeneic islets. Diabetes Technol. Ther. 5(4):653–663; 2003.
24. Kinnaird, T.; Stabile, E.; Burnett, M. S.; Lee, C. W.; Barr, S.; Fuchs, S.; Epstein, S. E. Marrow-derived stromal cells express genes encoding a broad spectrum of arteriogenic cytokines and promote in vitro and in vivo arteriogenesis through paracrine mechanisms. Circ. Res. 94(5):678–685; 2004.
25. Kinnaird, T.; Stabile, E.; Burnett, M. S.; Shou, M.; Lee, C. W.; Barr, S.; Fuchs, S.; Epstein, S. E. Local delivery of marrow-derived stromal cells augments collateral perfusion through paracrine mechanisms. Circulation 109(12):1543–1549; 2004.
26. Kisiday, J. D.; Hale, B. W.; Almodovar, J. L.; Lee, C. M.; Kipper, M. J.; Wayne McIlwraith, C.; Frisbie, D. D. Expansion of mesenchymal stem cells on fibrinogen-rich protein surfaces derived from blood plasma. J. Tissue Eng. Regen. Med. 5(8):600–611; 2011.
27. Klock, G.; Pfeffermann, A.; Ryser, C.; Grohn, P.; Kuttler, B.; Hahn, H. J.; Zimmermann, U. Biocompatibility of mannuronic acid-rich alginates. Biomaterials 18(10):707–713; 1997.
28. Kloxin, A. M.; Kloxin, C. J.; Bowman, C. N.; Anseth, K. S. Mechanical properties of cellularly responsive hydrogels and their experimental determination. Adv. Mater. 22(31):3484–3494; 2010.
29. Kunduzova, O. R.; Bianchi, P.; Pizzinat, N.; Escourrou, G.; Seguelas, M. H.; Parini, A.; Cambon, C. Regulation of JNK/ERK activation, cell apoptosis, and tissue regeneration by monoamine oxidases after renal ischemia–reperfusion. FASEB J. 16(9):1129–1131; 2002.
30. Kuo, C. K.; Ma, P. X. Ionically crosslinked alginate hydrogels as scaffolds for tissue engineering: Part 1. Structure, gelation rate and mechanical properties. Biomaterials 22(6):511–521; 2001.
31. Landa, N.; Miller, L.; Feinberg, M. S.; Holbova, R.; Shachar, M.; Freeman, I.; Cohen, S.; Leor, J. Effect of injectable alginate implant on cardiac remodeling and function after recent and old infarcts in rat. Circulation 117(11):1388–1396; 2008.
32. Leor, J.; Gerecht, S.; Cohen, S.; Miller, L.; Holbova, R.; Ziskind, A.; Shachar, M.; Feinberg, M. S.; Guetta, E.; Itskovitz-Eldor, J. Human embryonic stem cell transplantation to repair the infarcted myocardium. Heart 93(10):1278–1284; 2007.
33. Leor, J.; Tuvia, S.; Guetta, V.; Manczur, F.; Castel, D.; Willenz, U.; Petnehazy, O.; Landa, N.; Feinberg, M. S.; Konen, E.; Goitein, O.; Tsur-Gang, O.; Shaul, M.; Klapper, L.; Cohen, S. Intracoronary injection of in situ forming alginate hydrogel reverses left ventricular remodeling after myocardial infarction in Swine. J. Am. Coll. Cardiol. 54(11):1014–1023; 2009.
34. Maurel, A.; Azarnoush, K.; Sabbah, L.; Vignier, N.; Le Lorc'h, M.; Mandet, C.; Bissery, A.; Garcin, I.; Carrion, C.; Fiszman, M.; Bruneval, P.; Hagege, A.; Carpentier, A.; Vilquin, J. T.; Menasche, P. Can cold or heat shock improve skeletal myoblast engraftment in infarcted myocardium? Transplantation 80(5):660–665; 2005.
35. Mendes, J. B.; Campos, P. P.; Ferreira, M. A.; Bakhle, Y. S.; Andrade, S. P. Host response to sponge implants differs between subcutaneous and intraperitoneal sites in mice. J. Biomed. Mater. Res. B Appl. Biomater. 83(2):408–415; 2007.
36. Mias, C.; Trouche, E.; Seguelas, M. H.; Calcagno, F.; Dignat-George, F.; Sabatier, F.; Piercecchi-Marti, M. D.; Daniel, L.; Bianchi, P.; Calise, D.; Bourin, P.; Parini, A.; Cussac, D. Ex vivo pretreatment with melatonin improves survival, proangiogenic/mitogenic activity, and efficiency of mesenchymal stem cells injected into ischemic kidney. Stem Cells 26(7):1749–1757; 2008.
37. Moustafa, T.; Girod, S.; Tortosa, F.; Li, R.; Sol, J. C.; Rodriguez, F.; Bastide, R.; Lazorthes, Y.; Sallerin, B. Viability and functionality of bovine chromaffin cells encapsulated into alginate-PLL microcapsules with a liquefied inner core. Cell Transplant. 15(2):121–133; 2006.
38. Muller-Ehmsen, J.; Whittaker, P.; Kloner, R. A.; Dow, J. S.; Sakoda, T.; Long, T. I.; Laird, P. W.; Kedes, L. Survival and development of neonatal rat cardiomyocytes transplanted into adult myocardium. J. Mol. Cell. Cardiol. 34(2):107–116; 2002.
39. Neuhuber, B.; Swanger, S. A.; Howard, L.; Mackay, A.; Fischer, I. Effects of plating density and culture time on bone marrow stromal cell characteristics. Exp. Hematol. 36(9):1176–1185; 2008.
40. Nguyen, V. B.; Wang, C. X.; Thomas, C. R.; Zhang, Z. Mechanical properties of single alginate microspheres determined by microcompression and finite element modelling. Chem. Eng. Sci. 64(5):821–829; 2009.
41. Noort, W. A.; Feye, D.; Van Den Akker, F.; Stecher, D.; Chamuleau, S. A.; Sluijter, J. P.; Doevendans, P. A. Mesenchymal stromal cells to treat cardiovascular disease: Strategies to improve survival and therapeutic results. Panminerva Med. 52(1):27–40; 2010.
42. Orive, G.; Carcaboso, A. M.; Hernandez, R. M.; Gascon, A. R.;Pedraz, J. L. Biocompatibility evaluation of different alginates and alginate-based microcapsules. Biomacromolecules 6(2):927–931; 2005.
43. Orive, G.; Ponce, S.; Hernandez, R. M.; Gascon, A. R.; Igartua, M.; Pedraz, J. L. Biocompatibility of microcapsules for cell immobilization elaborated with different type of alginates. Biomaterials 23(18):3825–3831; 2002.
44. Orive, G.; Tam, S. K.; Pedraz, J. L.; Halle, J. P. Biocompatibility of alginate-poly-L-lysine microcapsules for cell therapy. Biomaterials 27(20):3691–3700; 2006.
45. Pittenger, M. F.; Martin, B. J. Mesenchymal stem cells and their potential as cardiac therapeutics. Circ. Res. 95(1):9–20; 2004.
46. Ponce, S.; Orive, G.; Hernandez, R. M.; Gascon, A. R.; Canals, J. M.; Munoz, M. T.; Pedraz, J. L. In vivo evaluation of EPO-secreting cells immobilized in different alginate-PLL microcapsules. J. Control. Release 116(1):28–34; 2006.
47. Purcell, E. K.; Singh, A.; Kipke, D. R. Alginate composition effects on a neural stem cell-seeded scaffold. Tissue Eng. Part C Methods 15(4):541–550; 2009.

48. Reinecke, H.; Zhang, M.; Bartosek, T.; Murry, C. E. Survival, integration, and differentiation of cardiomyocyte grafts: A study in normal and injured rat hearts. Circulation 100(2):193–202; 1999.
49. Simons, M. Angiogenesis: Where do we stand now? Circulation 111(12):1556–1566; 2005.
50. Simpson, N. E.; Stabler, C. L.; Simpson, C. P.; Sambanis, A.; Constantinidis, I. The role of the $CaCl_2$-guluronic acid interaction on alginate encapsulated betaTC3 cells. Biomaterials 25(13):2603–2610; 2004.
51. Stabler, C.; Wilks, K.; Sambanis, A.; Constantinidis, I. The effects of alginate composition on encapsulated betaTC3 cells. Biomaterials 22(11):1301–1310; 2001.
52. Sui, R.; Liao, X.; Zhou, X.; Tan, Q. The current status of engineering myocardial tissue. Stem Cell Rev. 7(1):172–180; 2010.
53. Suuronen, E. J.; Kuraitis, D.; Ruel, M. Improving cell engraftment with tissue engineering. Semin. Thorac. Cardiovasc. Surg. 20(2):110–114; 2008.
54. Tambara, K.; Sakakibara, Y.; Sakaguchi, G.; Lu, F.; Premaratne, G. U.; Lin, X.; Nishimura, K.; Komeda, M. Transplanted skeletal myoblasts can fully replace the infarcted myocardium when they survive in the host in large numbers. Circulation 108 Suppl 1:II259–263; 2003.
55. Tang, J.; Xie, Q.; Pan, G.; Wang, J.; Wang, M. Mesenchymal stem cells participate in angiogenesis and improve heart function in rat model of myocardial ischemia with reperfusion. Eur. J. Cardiothorac. Surg. 30(2):353–361; 2006.
56. Tang, Y. L.; Zhao, Q.; Zhang, Y. C.; Cheng, L.; Liu, M.; Shi, J.; Yang, Y. Z.; Pan, C.; Ge, J.; Phillips, M. I. Autologous mesenchymal stem cell transplantation induce VEGF and neovascularization in ischemic myocardium. Regul. Pept. 117(1):3–10; 2004.
57. Toma, C.; Pittenger, M. F.; Cahill, K. S.; Byrne, B. J.; Kessler, P. D. Human mesenchymal stem cells differentiate to a cardiomyocyte phenotype in the adult murine heart. Circulation 105(1):93–98; 2002.
58. Trouche, E.; Fullana, S. G.; Mias, C.; Ceccaldi, C.; Tortosa, F.; Seguelas, M. H.; Calise, D.; Parini, A.; Cussac, D.; Sallerin, B. Evaluation of alginate microspheres for mesenchymal stem cells engraftment on solid organ. Cell Transplant. 19(12):1623–1633; 2010.
59. Wang, L.; Shelton, R. M.; Cooper, P. R.; Lawson, M.; Triffitt, J. T.; Barralet, J. E. Evaluation of sodium alginate for bone marrow cell tissue engineering. Biomaterials 24(20):3475–3481; 2003.
60. Weir, M. D.; Xu, H. H. Human bone marrow stem cell-encapsulating calcium phosphate scaffolds for bone repair. Acta Biomater. 6(10):4118–4126; 2010.
61. Westrich, J.; Yaeger, P.; He, C.; Stewart, J.; Chen, R.; Seleznik, G.; Larson, S.; Wentworth, B.; O'Callaghan, M.; Wadsworth, S.; Akita, G.; Molnar, G. Factors affecting residence time of mesenchymal stromal cells (MSC) injected into the Myocardium. Cell Transplant. 19(8):937–948; 2010.
62. Wollert, K. C.; Drexler, H. Clinical applications of stem cells for the heart. Circ. Res. 96(2):151–163; 2005.
63. Yagi, H.; Soto-Gutierrez, A.; Parekkadan, B.; Kitagawa, Y.; Tompkins, R. G.; Kobayashi, N.; Yarmush, M. L. Mesenchymal stem cells: Mechanisms of immunomodulation and homing. Cell Transplant. 19(6):667–679; 2010.
64. Yu, J.; Christman, K. L.; Chin, E.; Sievers, R. E.; Saeed, M.; Lee, R. J. Restoration of left ventricular geometry and improvement of left ventricular function in a rodent model of chronic ischemic cardiomyopathy. J. Thorac. Cardiovasc. Surg. 137(1):180–187; 2009.
65. Yu, J.; Gu, Y.; Du, K. T.; Mihardja, S.; Sievers, R. E.; Lee, R. J. The effect of injected RGD modified alginate on angiogenesis and left ventricular function in a chronic rat infarct model. Biomaterials 30(5):751–756; 2009.
66. Zhu, J.; Sabharwal, T.; Kalyanasundaram, A.; Guo, L.; Wang, G. Topographic mapping and compression elasticity analysis of skinned cardiac muscle fibers in vitro with atomic force microscopy and nanoindentation. J. Biomech. 42(13):2143–2150; 2009.